

Observation of a Large Current on the Cyclic Voltammetry of Acylaminoferrocenes in the Solid State: An Efficient Electron-Transfer Pathway through Continuous NH···O=C Hydrogen-Bond Chains and π-Conjugation

Taka-aki Okamura, Keiko Sakauye, Mototsugu Doi, Hitoshi Yamamoto, Norikazu Ueyama,* and Akira Nakamura[1]

Department of Macromolecular Science, Graduate School of Science, Osaka University, Toyonaka, Osaka 560-0043

[1]OM Research, 7-2-1308 Minami Ogimachi, Kita-ku, Osaka 530-0052

Received December 14, 2004; E-mail: ueyama@chem.sci.osaka-u.ac.jp

A series of crystal structures of acylaminoferrocenes, [$(C_5H_5)Fe(C_5H_4NHCOR)$] (R = CH_3 (**1**), CH_2CH_3 (**2**), *t*-Bu (**3**), and CF_3 (**4**)) revealed an unusually delicate dependence of the alkyl substituent structure on electron transfer through NH···O=C bonding and π-conjugation. The presence of strong intermolecular NH···O=C hydrogen bonds in the crystal was established by X-ray, IR, and CRAMPS. Compounds **1** and **2** are without steric or electrostatic hindrance, and both exhibit continuous and strong hydrogen-bond chains, or an effective π-electrons system. However, the hydrogen-bond chains in **3** and **4** are weak, or broken, by the bulkiness of *t*-Bu or the electrostatic repulsion of CF_3. Solid-state cyclic voltammograms of **1**–**4** have revealed the electrochemical processes, which are critically dependent on the array and the strength of the hydrogen bonds. Although both **3** and **4** show typical reversible cyclic voltammograms, **1** and **2** exhibit irreversible redox behaviors and remarkably large current values, which indicate the presence of an effective electron transfer through the continuous hydrogen-bond chains.

Extensively conjugated organic systems or polynuclear metal coordination systems are the most promising candidate to develop novel conductive or semi-conductive materials. Many inorganic polymers have been investigated for this purpose. Polynuclear σ- or π-conjugated ferrocene derivatives connected by various linkages, especially, are well-known by concerning their ease of chemical modification, good solubility, satisfactory redox stability, and potential utilities, leading to various other physical applications. Poly(ferrocenylsilane)s have been known to show a semi-conductivity through a conjugated pathway after I_2- or TCNQ-doping. Partially oxidized polynuclear ferrocene derivatives are found in a mixed-valence state, and show intramolecular electron transfer in solution. However, the electron transfer is limited within several metal centers because the conjugation is broken at many points by the rotation around the bridging $-SiR_2-$ (R = alkyl) moiety.[1] Crystal engineering using hydrogen bonds presents us with an infinite conjugation chain, though it is limited by the crystal size. Various arrays of organic[2–7] and inorganic[8,9] compounds have been reported. We present here, the crystal structures of redox-active acylaminoferrocenes (Fc-NHCOR, Fc = ferrocenyl) having the intermolecular hydrogen bonds, and we describe the relationships between the strength and electron-transfer capability.

Acylaminoferrocenes form stronger NH···O=C hydrogen bonds than the corresponding carbamoyl derivatives (FcCONHR), as mentioned in a previous paper.[10] When amide NH is directly connected to a Cp ring, the electron on the lone pair of the amide NH is delocalized to the Cp ring through π-conjugation, which results in an increase of the protonic acidity of NH or the capacity for hydrogen bonding.[11] Indeed, [$Fe(C_5H_4CONHCH_3)_2$] has no NH···O=C hydrogen bond in the crystal despite the presence of amide groups.[12] However, applications had been limited in FcCONHR because of the difficulty of synthesizing aminoferrocene until the recent work,[13] and an improved synthetic procedure[14] has been known. *N*-Alkyl- or *N*-aryl-carbamoylferrocenes, [FcCONHR] (R = alkyl or aryl group), have been reported as substrate receptors that recognize anions by using intermolecular hydrogen bonds.[15–17] Recently, some acylaminoferrocene derivatives have been reported.[13,18]

The synthesis of acetylaminoferrocene has been known from long ago,[19] and recently its structure has been reported, but it shows an unacceptably large *R*1 factor (15.8%), which must be because of an incorrect solution. Here, we report on the structures of a series of acylaminoferrocenes and the formation of intermolecular hydrogen bonds in the solid state; we estimated the strength of the hydrogen bonds using X-ray, IR, ^{1}H NMR, and electrochemical analysis. As we reported previously, the variation of R in the acylamino (RCONH–) group effectively and successfully controls the strength of the hydrogen bond.[20–24]

Electrochemical measurements, especially cyclic voltammetry in the solid state surrounded by aqueous medium, are useful techniques for the analysis of insoluble materials (e.g., Prussian Blue [PB]),[25–30] as well as for the analysis of unstable compounds by dissociation of the ligand or total decomposition in solution.[31] The shape of cyclic voltammograms in the

Published on the web July 1, 2005; DOI 10.1246/bcsj.78.1270

solid state has been interpreted as a diffusion-controlled redox process, just as is true for ordinary ones in solution. Ferrocene in the solid state using a carbon-paste electrode typically shows a reversible redox Fe^{III}/Fe^{II} couple, just as in solution, although the current value is very small because of the limited movement of molecules, or its low solubility in water.[31] On the other hand, PB shows a larger current value that is enabled by the diffusion of potassium ions in the PB lattice. The current values and the redox process are considered to represent the mobility of electrons and ions or the electronic interaction in the solid state. If electrons move through conjugated hydrogen-bond chains in the solid state, the electric current should be accelerated, compared with a diffusion-controlled process. In this paper, we discuss the relationship between the strength of the hydrogen bond and the ease of electron transfer in the solid state.

Experimental

Materials. All procedures, except for column chromatography, were performed under an argon atmosphere. The carbon paste and electrode for electrochemical measurements were purchased from BAS Inc. All solvents were dried and distilled under argon before use. The other reagents were commercially available.

Acetylaminoferrocene (1). This compound was prepared by a literature method.[19] Single crystals for X-ray analysis were prepared by recrystallization from ethyl acetate. ^{1}H NMR (chloroform-d_1): δ 6.51 (s, 1H), 4.56 (t, 2H), 4.16 (s, 5H), 3.99 (t, 2H), 2.06 (s, 3H). Anal. Found: C, 59.29; H, 5.32; N, 5.86%. Calcd for $C_{12}H_{13}NOFe$: C, 59.29; H, 5.39; N, 5.76%.

Preparation of Aminoferrocene. Acetylaminoferrocene (100 mg, 0.41 mmol) was suspended in 6 M HCl aq (20 mL) and heated at 80 °C for 1 h. Insoluble materials were removed by filtration. The obtained clear filtrate was washed with diethyl ether twice. The acidic solution was neutralized by $NaHCO_3$ and diethyl ether was added. The ethereal layer was washed with a NaCl-saturated aqueous solution, dried over Na_2SO_4, and concentrated. The crude product was purified by column chromatography using silica gel and ethyl acetate as the eluent. Yield 46 mg (56%). ^{1}H NMR (chloroform-d_1): δ 4.10 (s, 5H), 4.00 (t, 2H), 3.85 (t, 2H), 2.56 (s, 2H). Anal. Found: C, 59.78; H, 5.36; N, 6.73%. Calcd for $C_{10}H_{11}NFe$: C, 59.74; H, 5.51; N, 6.97%.

Propionylaminoferrocene (2). Aminoferrocene (0.31 g, 1.5 mmol) and triethylamine (0.2 mL, 1.7 mmol) were dissolved in CH_2Cl_2 (10 mL). Propionyl chloride (0.2 mL, 1.7 mmol) was added to the solution cooling in an ice bath. After stirring overnight, water (30 mL) and diethyl ether (20 mL) were added to the reaction mixture. The product was extracted with ethyl acetate. The combined organic layer was washed successively with 2% HCl aq, sat. NaCl aq, 4% $NaHCO_3$ aq, and sat. NaCl aq, dried over Na_2SO_4, and concentrated to dryness in vacuo. The crude product was recrystallized from hot ethyl acetate to give orange needles. Single crystals for X-ray analysis were prepared by recrystallization from propionitrile. Yield 0.36 g (92%). ^{1}H NMR (chloroform-d_1): δ 6.41 (s, 1H), 4.58 (t, 2H), 4.15 (s, 5H), 3.99 (t, 2H), 2.27 (q, 2H), 1.22 (t, 3H). Anal. Found: C, 60.23; H, 5.93; N, 5.22%. Calcd for $C_{13}H_{15}NOFe$: C, 60.73; H, 5.88; N, 5.45%.

Pivaloylaminoferrocene (3). The compound was synthesized by a similar method as described for **2**. Recrystallization from hot ethyl acetate gave orange needles in 74% yield. ^{1}H NMR (chloroform-d_1): δ 6.62 (s, 1H), 4.61 (t, 2H), 4.13 (s, 5H), 3.98 (t, 2H), 1.27 (s, 9H). Anal. Found: C, 62.98; H, 6.52; N, 4.97%. Calcd for $C_{15}H_{19}NOFe$: C, 63.18; H, 6.72; N, 4.91%.

Trifluoroacetylaminoferrocene (4). Aminoferrocene (0.50 g, 2.5 mmol) was dissolved in CH_2Cl_2 (10 mL), and trifluoroacetic anhydride (0.8 mL, 5.7 mmol) was added to the solution. After stirring overnight at room temperature, crushed ice was added to a solution cooling in an ice bath, and the solvent was evaporated under reduced pressure. The residue was dissolved in ethyl acetate and the solution was washed with sat. NaCl aq, dried over Na_2SO_4, and concentrated. The crude product was purified by column chromatography using silica gel and ethyl acetate as the eluent. Recrystallization from ethyl acetate gave orange plates. Yield 0.64 g (87%). ^{1}H NMR (chloroform-d_1): δ 7.32 (s, 1H), 4.59 (t, 2H), 4.13 (s, 5H), 4.04 (t, 2H). Anal. Found: C, 47.99; H, 3.68; N, 4.39%. Calcd for $C_{12}H_{10}NOF_3Fe$: C, 48.52; H, 3.39; N, 4.72%.

Physical Measurements. ^{1}H NMR spectra in solution were taken on a Jeol GSX-400 spectrometer in $CDCl_3$ or CD_2Cl_2. Solid-state ^{1}H NMR spectra using the CRAMPS (combined rotation and multipulse spectroscopy) technique were taken on a Chemmagnetics CMX-300. MREV-8 pulse sequence and 3 kHz spinning were used to detect amide NH protons. Tetrakis(trimethylsilyl)silane (TTMS) was used as an internal standard at 0.2 ppm from TMS. IR spectra were recorded on a Jasco FT/IR 8300 spectrometer. Samples were prepared as 10 mM CH_2Cl_2 solutions or as KBr pellets. Cyclic voltammograms were obtained by BAS 100B/W in solution and in the solid state using a three-electrode method. The solution samples were prepared as a 2.5 mM CH_2Cl_2 solution, including 0.2 M tetrabutylammonium perchlorate as a supporting electrolyte. The solid samples were prepared as follows. The electrode body and carbon paste were purchased from Bioanalytical Systems, Inc. (BASi). The carbon paste was mixed well with 5 wt % of ferrocene derivatives and filled into an electrode body with metallic rod, which was used as a working electrode. The measurements were performed in an aqueous 0.1 M $NaClO_4$ solution. The scan rate was 100 mV/s for the solution and 50 mV/s for the solid state. The $E_{1/2}$ value was determined using the SCE electrode as a reference at room temperature.

Ab initio Calculations. The bond order of the hydrogen-bonded amide groups was calculated using a dimeric model. Two neighboring molecules forming an intermolecular NH···O=C hydrogen bond with each other were positioned for the dimeric model according to the atomic coordinates, determined by X-ray analysis. For **1** and **3**, which have two distinct molecules in the asymmetric unit, two kinds of dimeric models were used. Ab initio calculations (single point energy) were performed by Wavefunction Inc. SPARTAN (ver. 4.1.2) using 3-21G(*) basis set.

X-ray Data Collection and Structural Determination. Each of suitable crystals of $[(C_5H_5)Fe(C_5H_4NHCOR)]$ (R = CH_3 (**1**), CH_2CH_3 (**2**), *t*-Bu (**3**), and CF_3 (**4**)) was sealed in a glass capillary under an argon atmosphere. X-ray measurements were made at 23 °C on a Rigaku AFC5R (**1** and **4**) or AFC7R (**2** and **3**) diffractometer with graphite monochromated Mo Kα radiation (0.71069 Å) using the ω-2θ scan up to $2\theta_{max} = 55°$. The unit cell dimensions were refined with 25 reflections. The basic crystallographic parameters are listed in Table 1. Three standard reflections were chosen and monitored with every 150 reflections, and did not show any significant change. An absorption correction based on azimuthal scans of several reflections was applied for **2** and **4**. The structures were solved by a direct method (SHELXS 86)[32] using the teXsan crystallographic software package of the Molecular Structure Corp. The positions of one *t*-Bu group in **3** were disordered. The multiplicity for the major position (C107–C109) was converged to 0.511. All non-hydrogen atoms were refined

Table 1. Crystallographic Data for $[(C_5H_4NHCOR)Fe(C_5H_5)]$ (**1**–**4**)

R	CH_3 (**1**)	CH_2CH_3 (**2**)	*t*-Bu (**3**)	CF_3 (**4**)
Empirical formula	$C_{12}H_{13}NOFe$	$C_{13}H_{15}ONFe$	$C_{15}H_{19}ONFe$	$C_{12}H_{10}ONFeF_3$
Formula weight	243.09	257.11	285.17	297.06
Crystal system	monoclinic	monoclinic	orthorhombic	monoclinic
a/Å	5.9845(4)	9.033(3)	14.939(3)	15.344(1)
b/Å	7.520(6)	13.112(4)	18.097(3)	7.640(2)
c/Å	23.58(1)	10.158(5)	10.158(2)	10.202(1)
β/deg	92.93(4)	108.29(3)	90	109.043(7)
V/Å^3	1060(1)	1142.4(8)	2746.1(9)	1130.5(3)
Space group	$P2_1$	$P2_1/c$	$P2_12_12_1$	$P2_1/c$
Z	4	4	8	4
D_{calc}/g cm^{-3}	1.523	1.495	1.379	1.745
μ(Mo Kα)/mm^{-1}	1.390	1.295	1.085	1.358
No. of reflections	2621	2625	3542	2588
$R1[F_o^2 > 2\sigma(F_o^2)]$	0.036	0.046	0.036	0.040
$wR2$	0.106	0.143	0.106	0.110
GOF	1.07	1.04	1.00	0.99

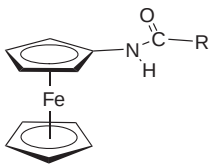

R = CH_3 (**1**), Et (**2**), *t*-Bu (**3**), CF_3 (**4**)

Chart 1.

anisotropically on F^2 by the full-matrix least-squares method (SHELXL97).[33] All hydrogen atoms were placed at the calculated positions. The final difference Fourier map showed no significant features. Atom scattering factors and dispersion corrections were taken from the International Table.[34] Crystallographic data have been deposited with Cambridge Crystallographic Data Centre: Deposition numbers CCDC 257497–257500 for **1**–**4**. Copies of the data can be obtained free of charge via http://www.ccdc.cam.ac.uk/conts/retrieving.html (or from the Cambridge Crystallographic Data Centre, 12, Union Road, Cambridge, CB2 1EZ, UK; Fax: +44 1223 336033; e-mail: deposit@ccdc.cam.ac.uk).

Results and Discussion

Synthesis. A series of acylaminoferrocenes, $[(C_5H_5)Fe(C_5H_4NHCOR)]$ (R = CH_3 (**1**), CH_2CH_3 (**2**), *t*-Bu (**3**), and CF_3 (**4**)) (Chart 1), was systematically synthesized to reveal the electrostatic and steric contributions to the hydrogen-bond formation. The smallest substituent, formyl group (R = H), was not used. The derivative exists as an equilibrium mixture of monomers and oligomers in solution, and does not give single crystals due to *cis* amide hydrogen-bonding bridge.[35]

Intermolecular NH···O=C Hydrogen Bonds in the Crystal. Compounds **1**–**4** were readily crystallized to form intermolecular NH···O=C hydrogen bonds. Hydrogen-bond chains in the crystal are shown as broken lines in Fig. 1. Both compounds **1** and **3** exhibit two crystallographically independent molecules in the asymmetric unit. Recently, the structure of **1** was reported, but the space group is $P2_1/n$ and the $R1$ factor is unacceptably large (15.8%),[18] a finding that must be the result of an incorrect solution. The selected bond length and

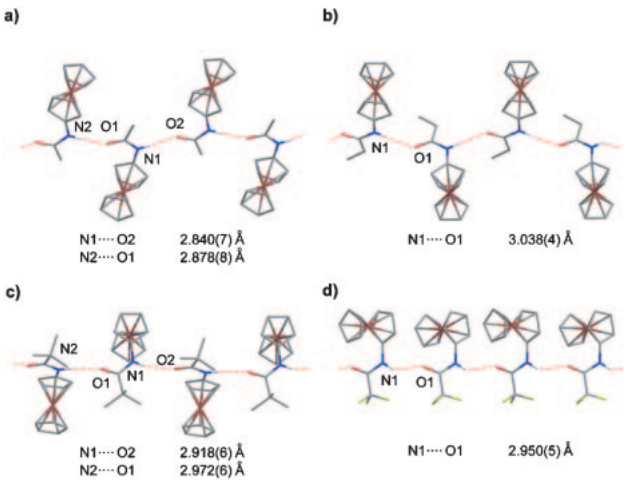

Fig. 1. One-dimensional NH···O=C hydrogen bond chain in $[(C_5H_5)Fe(C_5H_4NHCOR)]$ where R indicates a) CH_3 (**1**), b) CH_2CH_3 (**2**), c) *t*-Bu (**3**), and d) CF_3 (**4**).

angles are listed in Table 2. Conventional values of the bond lengths and the angles were found. The amide planes of **1** and **4** show high coplanarity (dihedral angles between two planes are 7.2° for **1** and 34.0° for **4**), and their hydrogen-bonding motifs exhibit the typical glide for **1** and translation for **4**, respectively.[36] On the other hand, the amide planes of **2** (85.2°) and **3** (86.8°) are mutually perpendicular. Semiempirical and ab initio calculations showed that the strength of the NH···O=C hydrogen bond, or the interaction energy between two hydrogen-bonding amide planes, is independent of the torsion angle(O)C–N–C(O)–N between the two amide planes.[37] Thus, we disregard the coplanarity of the two amide planes in any discussion about the strength of the hydrogen bond.

Taylor et al. have reported a geometrical analysis of the NH···O=C hydrogen bonds and a statistically significant tendency for hydrogen-bond formation.[38,39] We evaluated Taylor's geometrical parameters for the hydrogen bonds in **1**–**4**, and summarize the results in Table 3. The definitions of the parameters are represented in Fig. 2. All N–H bond dis-

Table 2. Selected Bond Length (Å) and Angles (deg) in $[(C_5H_5)Fe(C_5H_4NHCOR)]$

R	CH_3 (**1**)		CH_2CH_3 (**2**)	*t*-Bu (**3**)		CF_3 (**4**)
	molecule A	molecule B		molecule A	molecule B	
Fe–C mean	2.024	2.042	2.047	2.040	2.028	2.033
Fe–Cp mean	1.641	1.656	1.655	1.650	1.649	1.650
C11–N1–C16–O1 (C21–N2–O26–O2)[a]	−1.5(9)	1.6(11)	1.0(6)	−1.3(9)	3.2(9)	−1.8(7)
C16–N1–C11–C12 (C26–N2–C21–C22)[a]	−17.6(10)	−159.3(6)	−3.3(6)	−172.2(6)	179(6)	29.5(6)
Cp–Cp′[b]	1.2	0.5	1.0	2.5	1.5	1.2
Cp–amide plane[c]	18.9	23.7	2.1	6.4	5.1	26.2

a) Parenthesis indicates the numbering for molecule B. b) Dihedral angle between two Cp rings in a molecule. c) Dihedral angle between an amide plane and the adjacent Cp ring.

Table 3. The Distances and Angles of $[(C_5H_5)Fe(C_5H_4NHCOR)]$[a]

R	CH_3 (**1**)	CH_2CH_3 (**2**)	*t*-Bu (**3**)	CF_3 (**4**)	reported value[b]
NH···O (Å)	1.812 1.866	2.059	1.960 1.990	2.088	1.869 ± 0.108
N···O (Å)	2.840(7) 2.878(8)	3.038(4)	2.918(6) 2.972(6)	2.950(5)	2.850 ± 0.089
NH···O (deg)	175.7 166.5	157.8	153.5 158.3	139.8	161.3 ± 11.6
θ	83.6 86.3	87.4	88.4 86.2	81.9	
ϕ	56.5 55.0	50.1	69.8 75.5	63.0	

a) NH bond distances are normalized to 1.030 Å which is the standard value determined by neutron diffraction.[38,39] b) Ref. 38.

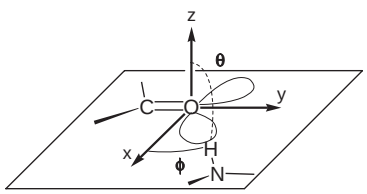

Fig. 2. Illustration for the angles defined by the orientation of amide NH toward the lone pair on carbonyl group.[38]

tances were normalized to 1.030 Å, which is the reported mean value determined by neutron diffraction. The statistical mean values of 57 observations have been reported, (i.e., NH···O=C = 1.869 ± 0.108 Å, N···O = 2.850 ± 0.089 Å, and N–H···O = $161.3 \pm 11.6°$).[38] The two NH···O=C distances (1.812 and 1.866 Å) of **1** are significantly shorter than the reported mean value. The NH···O=C distances of **2** (2.059 Å) and **3** (1.960, 1.990 Å) are slightly longer. The calculated optimal NH···O=C distances have been reported to be 1.94 Å in the gas phase and 2.20 Å in aqueous solution.[37] Because the distances for **2** and **3** are close to these values, they are considered to form effective NH···O=C hydrogen bonds. When the H···O distance is short, the NH···O=C angle has a tendency to increase, thereby avoiding an N···O non-bonded interaction. Actually, the mean of the distribution of the reported NH···O=C angles is 161.2(3)°.[38] The extended conformation (i.e. NH···O=C = 180°) is favored and supported by theoretical calculations.[37] The wider angle (175.7°) of **1** reflects the corresponding shorter N···O contact (2.840(9) Å). The linearity of NH···O=C suggests that the order of the strength of hydrogen bond is **1** > **2** > **3** > **4**.

In an ideal NH···O=C hydrogen bond, the θ and ϕ values equal 90° and 30°, respectively; that is, the hydrogen atom is placed on the lobe of the sp^2 lone-pair of the carbonyl group.[39] Actually, statistics have indicated a significant tendency for hydrogen bonds to form near the idealized sp^2 lone-pair direction (i.e., $77° < \theta \leq 90°$, $20° < \phi < 30°$).[38,39] Theoretical calculations have revealed the optimal angles to be θ = ca. 50° and $\phi = 90°$.[37] If the discussion is limited to the contribution of θ and ϕ, the observed trend for the hydrogen bonds is **2** > **1** > **4** > **3**. Because many competitive geometrical factors contribute to the strength of the hydrogen bonds, we were unable to determine the exact order of the strength. At the very least, we can conclude here that the hydrogen bonds in **1** are significantly and remarkably strong.

IR Spectra. The IR spectral data of **1**–**4** in the amide region are summarized in Table 4. In a dilute CH_2Cl_2 solution, only non-hydrogen bonding, (i.e. the "free" amide group) was found. The differences in the wavenumber of the absorption maxima are ascribed to an inductive effect of the substituent, R. In the solid state, the presence of two sets of distinct ν(NH) and ν(C=O) bands of **1** with the 1:1 ratio of the intensity is attributed to the two unequivalent molecules in the crystal. The ν(NH) at the lowest wavenumber (3211 cm^{-1}) is as-

Table 4. IR Spectral Data (cm^{-1}) of $[(C_5H_5)Fe(C_5H_4NHCOR)]$

R	in CH_2Cl_2		in the Solid state			
	ν(NH)	ν(C=O)	ν(NH)	ν(C=O)	$\Delta\nu$(NH)[a)]	$\Delta\nu$(C=O)[b)]
CH_3	3432	1687	3259, 3211	1654	173, 221	33
CH_2CH_3	3435	1688	3295, 3210	1665	140, 225	23
t-Bu	3455	1678	3301	1653	154	25
CF_3	3417	1738	3328	1718	89	20

a) $\Delta\nu(NH) = \nu(NH)_{solid} - \nu(NH)_{solution}$. b) $\Delta\nu(C{=}O) = \nu(C{=}O)_{solid} - \nu(C{=}O)_{solution}$.

signable to the amide NH with the shortest NH···O=C contact (1.812 Å). Complex **2** also showed two distinct ν(NH) at 3295 (major) and 3210 cm^{-1} (minor) with an integral ratio of 3:1. However, we detected no distinct molecules in the crystal by X-ray diffraction analysis. This finding suggests the presence of two or more distinct amide groups on the time scale of IR, which are averaged and could not be distinguished by X-ray diffraction analysis. We evaluated the strength of the hydrogen bonds in the solid state from $\Delta\nu$(NH). The values of ν(NH) and $\Delta\nu$(NH) suggest the strength of the hydrogen bonds to be in the order of **1** > **2** ≥ **3** > **4**.

^{1}H NMR Spectra. The chemical shifts of the amide NH signals in dichloromethane-d_2 and in the solid state are summarized in Table 5. ^{1}H NMR spectra in the solid state (i.e., CRAMPS) are shown in Fig. 3. In dichloromethane-d_2 solution, amide NH protons of **1**–**4** were observed at 6.4–7.3 ppm. These amides are free under this condition, and the differences of the chemical shifts are because of the inductive effect of the substituents, such as those found in the IR spectra. In the solid state, two distinct signals were found in **1**, **2**, and **3**. For **1** and **3**, two independent molecules exist in the crystal, as established by the X-ray analysis. However, **2** crystallographically exhibits only one kind of molecule. As described in the IR spectra, **2** shows two distinct ν(NH) bands. The split peaks in ^{1}H NMR also suggest the presence of two kinds of amide groups that are indistinguishable from each other by X-ray analysis.

Table 5. Chemical Shift (δ) of the Amide NH Proton of $[(C_5H_5)Fe(C_5H_4NHCOR)]$

R	in CD_2Cl_2	in the Solid state		Differences	
CH_3	6.6	10.6	9.4	4.0	2.8
CH_2CH_3	6.4	9.8	8.6	3.4	2.2
t-Bu	6.6	10.0	8.8	3.4	2.2
CF_3	7.3	9.2		1.9	

The peak at the lowest field (10.6 ppm) corresponds to the strongest NH···O=C hydrogen bond in **1**. The small difference (1.9 ppm) of the chemical shift for **4** between the solid state and in solution agrees with the small $\Delta\nu$(NH) value (89 cm^{-1}). In the ^{1}H NMR spectra, a trend of the strength of the hydrogen bond, **1** > **2** = **3** > **4**, was found. The difference be-

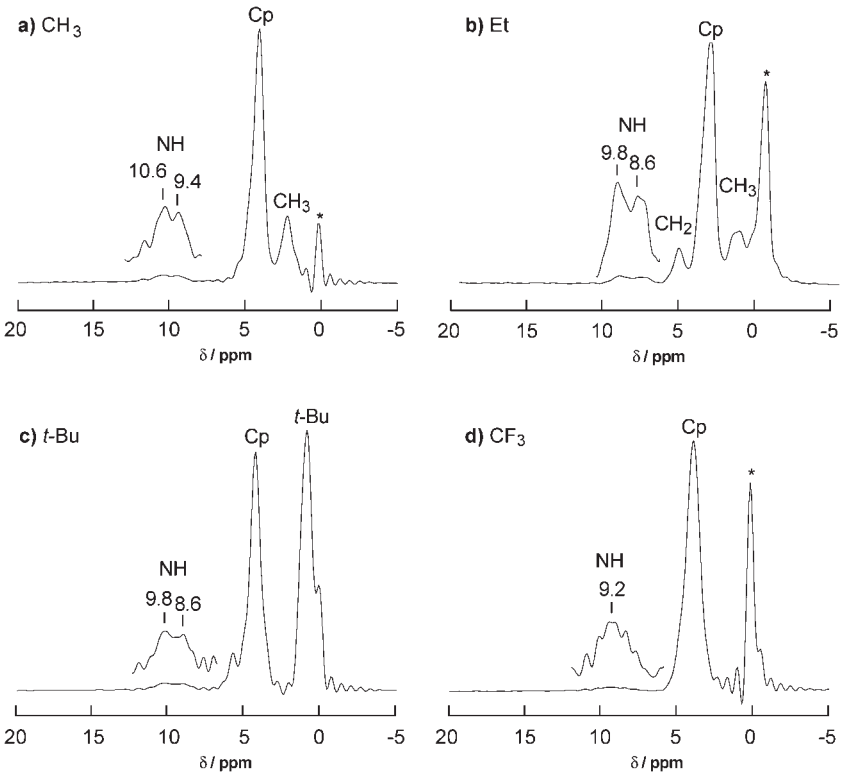

Fig. 3. ^{1}H NMR spectra (CRAMPS) of **1**–**4** in the solid state. * denotes the peaks of TTMS (tetrakis(trimethylsilyl)silane as standard).

tween **2** and **3**, as found in the IR spectra, was not discriminated by ^{1}H NMR.

Recently, CRAMPS has come to one of the most powerful techniques used in detecting hydrogen bonds. In some cases, however, disagreements between the CRAMPS and the IR data can occur. These discordant results have been attributed to the dependency of IR on the transition dipole moment and the significant differential time scale between the two methods.[40]

Cyclic Voltammograms. Each compound **1**–**4** exhibits a reversible redox couple in dichloromethane. The $E_{1/2}$ values are found at 0.34 V (vs SCE) for **1**–**3**, and 0.49 V for **4**. Under the same condition, ferrocene shows a redox couple at 0.48 V. The redox potentials of the ferrocene derivatives have been reported to be controlled by the electronic effects of the substituents The values show a good correlation with the Hammett substituent parameters, except for NH_2 and NHCOMe, as reported previously by Lever et al.[41] The unexpected negative shifts for **1**–**3**, of which the Hammett constants nearly equal 0, are considered to be caused by delocalization of the π-electron on the amide N to the adjacent Cp ring. The delocalization increases the acidity of the amide proton and its ability to form intermolecular NH···O=C hydrogen bonds.

Cyclic voltammograms of **1**–**4** in the solid state are shown in Fig. 4. Ferrocene shows a reversible redox couple at 0.26 V vs SCE under the same condition. Compounds **1** and **2** show an irreversible redox process and a large current value, although both **3** and **4** show a reversible couple with a small current value, as was found for ferrocene. The feature of the cyclic voltammograms was not significantly dependent on the method of the preparation (particle size, the extent of mixing, concentration of the sample, etc.). The difference must be caused by intermolecular electronic interactions in the crystal.

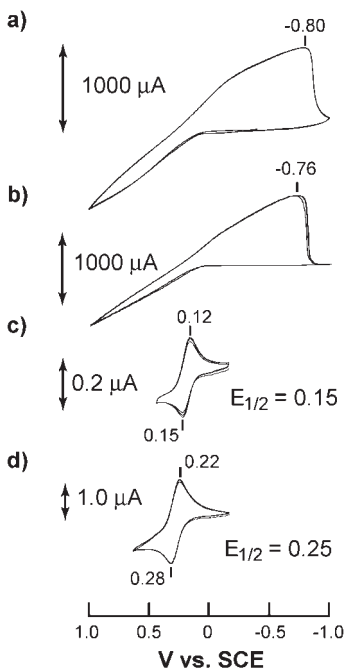

Fig. 4. Cyclic voltammograms of [$(C_5H_5)Fe(C_5H_4$-NHCOR)] in the solid state, where R indicates a) CH_3 (**1**), b) CH_2CH_3 (**2**), c) *t*-Bu (**3**), and d) CF_3 (**4**). The scans for **1** and **2** were started at −0.4 V and swept to the negative side (2 cycles).

In general, the redox behavior is influenced by several factors: (i) solubility of the sample in an aqueous medium, (ii) identity of the electrolyte, (iii) concentration of the sample in carbon paste, (iv) temperature, (v) scan rate, (vi) mobility of ions in the solid state, etc.[42,43] When ferrocene is oxidized to the ferrocenium cation, it becomes soluble in aqueous media. Previously, the diffusion-controlled redox behavior was believed to be induced by diffusion of the ferrocenium cation from carbon paste to an aqueous medium;[42] but this hypothesis has been disproved. Even when a completely water-insoluble solid was used during the redox process, a diffusion-controlled voltammetric process was observed. From this result, mass or ion transport has been considered to take place across the solid–solution interface at a sufficiently fast rate to observe a measurable current, and ions must diffuse within the solid to achieve its oxidation.[28,29] Especially, at a low scan rate, a diffusion-controlled process occurs in the thick layer of the solid. Thus, electron and ion transports within the solid are necessary.[29,42]

In the case of **1** and **2**, the observed large current values suggest the presence of a certain electron-transport mechanism that is different from those of **3** and **4**. Here, we propose a probable electron-transport process that occurs via intermolecular NH···O=C hydrogen bonds. In the case of Prussian blue (PB), the large current (∼1 mA) is caused by the diffusion of potassium ions through the PB lattice.[25]

In our case, electron transfer is considered to occur in the solid-carbon paste interface, as illustrated in Fig. 5. The redox reaction probably proceeds in the thick layer of the electrode. Even when the surface on the electrode was covered with pure carbon paste, an effective redox process was observed. In the ordinary case (i.e., for **3** and **4**), a molecule near the electrode (part of metallic rod) is electrochemically oxidized in the first step. The neighboring molecule then diffuses toward the electrode, and is then oxidized (step 2). Because the diffusion of a molecule is slower than that of the redox reaction, all of the redox-active species near the electrode are finally oxidized, resulting in a decrease of the current.

In the case of **1** and **2**, the situation is very different (Fig. 5c). These compounds form strong NH···O=C intermolecular hydrogen bonds, as established by X-ray diffraction analysis and spectral measurements in the crystal. Once a molecule near the electrode is oxidized (step 1), an electron on the neighboring molecule is then transferred to the oxidized molecule through the hydrogen bond (step 2). These molecules constitute a dimeric mixed-valence structure, Fe^{II}–$Fe^{III} \rightleftharpoons Fe^{III}$–$Fe^{II}$, connected by a stronger NH···O=C hydrogen bond than the Fe^{II}–Fe^{II} state, because the acidity of NH is increased by the inductive effect of the electron-deficient Fe(III) ion.

The observed electron transfer through the NH···O=C hydrogen bond is thus explained as fast electron transfer without diffusion control. In the first step of the oxidation process, molecules near the metallic rod are oxidized at an oxidation potential similar to that of **3** and **4**. The anodic current increases without any diffusion control, as shown in Fig. 4. In the oxidation process, the oxidized molecules are connected successively by very strong intermolecular NH···O=C hydrogen bonds to produce a cationic mixed-valence polymer (Fig. 5c, Eq. 1).

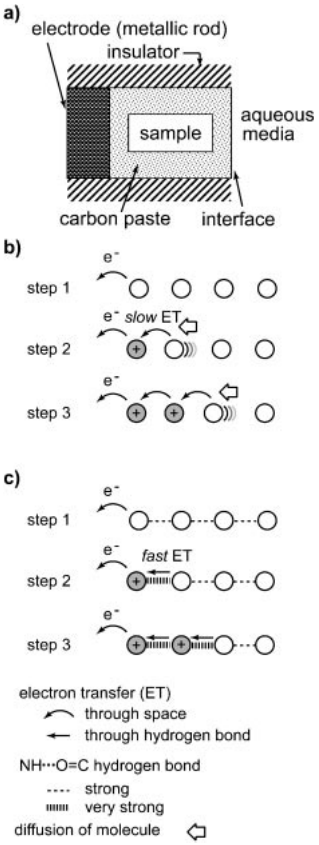

Fig. 5. Schematic representation of a) a carbon paste electrode including acylaminoferrocenes and the proposed oxidation process within the electrode for the cyclic voltammograms of b) **3** and **4** and c) **1** and **2** in the solid state.

$$\mathrm{Fe^{II}\cdots Fe^{II}\cdots Fe^{II}\cdots Fe^{II}\cdots Fe^{II}\cdots Fe^{II}\cdots} \xrightarrow{-2e^-} \mathrm{Fe^{III}\text{–}Fe^{III}\text{–}Fe^{II}\cdots Fe^{II}\cdots Fe^{II}\cdots Fe^{II}\cdots}. \quad (1)$$

During a cathodic scan, the current increases continuously and decreases sharply down to 0 A at approximately −0.8 V. This irreversible reduction process is explained as follows. In the reduction process, the fully oxidized hydrogen-bonded polymer is reduced near the metallic rod to form a mixed-valence polymer (Eq. 2). The reduction potential of the polymer must be more negative than that of the monomer when the majority is in the Fe^{II} state; for example, the associated mixed valence, Fe^{II}–Fe^{III}–Fe^{II}, is more difficult to be reduced than monomeric Fe^{III}. The stepwise reduction increases the population of Fe^{II} in the polymer. As mentioned above, hydrogen bonds in the Fe^{II} state are weaker than those in the Fe^{III} state. Thus, the reduction accompanies a weakening and dissociation of the hydrogen bonds, resulting in the formation of Fe^{II}-rich oligomers (Eq. 3), in which inducing reduction becomes increasingly difficult.

$$\cdots\text{–}\mathrm{Fe^{III}\text{–}Fe^{III}\text{–}Fe^{III}\text{–}Fe^{III}\text{–}Fe^{III}\text{–}Fe^{III}}\text{–}\cdots$$

fully oxidized polymer

$$\xrightarrow{e^-} \cdots\text{–}\mathrm{Fe^{II}\text{–}Fe^{III}\text{–}Fe^{III}\text{–}Fe^{III}\text{–}Fe^{III}\text{–}Fe^{III}}\text{–}\cdots, \quad (2)$$

partially reduced (mixed valent) polymer

$$\cdots\text{–}\mathrm{Fe^{II}\text{–}Fe^{III}\text{–}Fe^{III}\text{–}Fe^{II}\text{–}Fe^{III}\text{–}Fe^{II}}\text{–}\cdots \xrightarrow{e^-} \cdots\text{–}\mathrm{Fe^{II}\text{–}Fe^{III}\text{–}Fe^{II}} + \mathrm{Fe^{II}\text{–}Fe^{III}\text{–}Fe^{II}}\text{–}\cdots. \quad (3)$$

Fe^{II}-rich oligomers

During the cathodic sweep, potentially reducible Fe^{III} species remain in the oligomer at the reduction potential of monomeric Fe^{III}. Despite hydrogen bonds being weakened by the reduction, oligomeric structures probably remain at the reduction potential of a monomeric acylaminoferrocenium cation. Thus, the cathodic current slowly increases at the exceeded potential for the reduction of monomeric compounds. Finally, the partially oxidized oligomers are reduced all at once; that is, a multi-electron transfer occurs at a sufficiently negative potential (i.e., at approximately −0.8 V, as shown in Fig. 4 and Eq. 4). At ca. −0.80 V,

$$(\mathrm{Fe^{III}})_m\text{–}(\mathrm{Fe^{II}})_n \xrightarrow{me^-} (n+m)\ \mathrm{Fe^{II}}. \quad (4)$$

mixed valent oligomer ($n > m$) monomers

Competitive Intermolecular NH···S and NH···O=C Hydrogen Bond. To confirm the relationship between the presence of a strong intermolecular NH···O=C hydrogen bond chain and a large current value, we performed a cleavage of the hydrogen bond chain by addition of the ethanethiolate anion. Thus, the ethanethiolate anion was added to acetylaminoferrocene (**1**) in CH_2Cl_2 to form the intermolecular NH···S hydrogen bond, the existence of which was established by IR measurements; the mixture was then concentrated to dryness. The IR spectra of the residue were measured. As shown in Fig. 6, **1** exhibits two kinds of strong intermolecular NH···O=C hydrogen bonds. The addition of 1 equiv $(n\text{-Bu})_4$NSEt broke half of the NH···O=C bonds, and formed intermolecular NH···S hydrogen bonds. The resulting free ν(C=O) was observed at 1669 cm^{-1}. The corresponding cyclic votammogram showed a quasi-reversible redox process at $E_{1/2} = 0.16$ V vs SCE, and a slightly smaller current value (100 μA). After the addition of 10 equiv of thiolate, all amide groups were engaged in the intermolecular NH···S hydrogen bonds. The reversibility of the cyclic voltammogram increased, and the current decreased. This phenomenon was not caused by a simple electrolyte. When 10 equiv Ph_4PBr was used instead of $(n\text{-Bu})_4$NSEt, IR spectra and cyclic voltammograms showed similar features to the original ones. These results clearly indicate the formation of NH···S interrupts electron transfer through the intermolecular NH···O=C hydrogen bonds.

Theoretical Calculation of the Strength of NH···O=C Hydrogen Bonds. The electrochemical measurements demonstrated that the hydrogen bonds in **1** and **2** are stronger than those of **3** and **4**. This trend was found in the crystal data and the IR spectra. However, a significant difference of the strength of the hydrogen bonds was not detected between **2** and **3** based on the ^{1}H NMR and the IR spectra. The measurements evaluated the strength of the N–H bonds, or the electronic environment around the protons. However, the ^{1}H NMR and the IR spectra did not directly detect H···O bonds, nor did these methods estimate the strength of the bond. Because a direct evaluation of H···O bonds by spectral measurements is very difficult, we estimated the strength of the H···O bonds

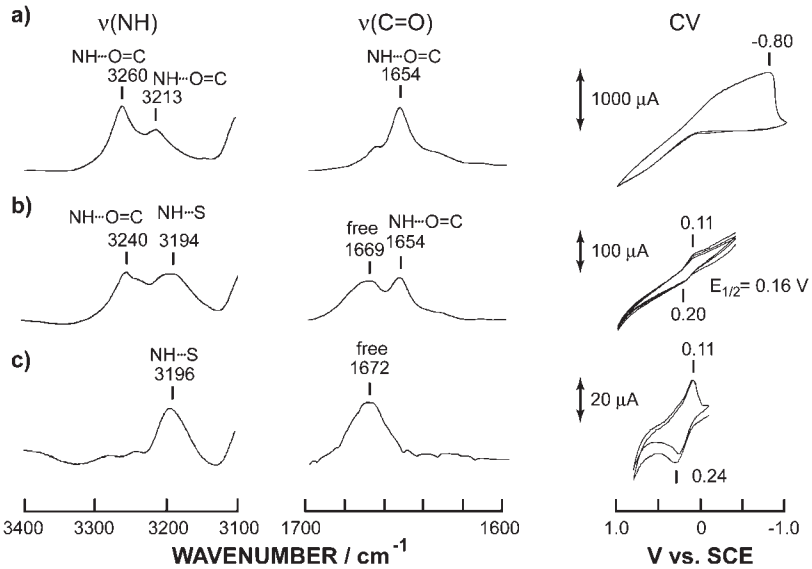

Fig. 6. IR spectra and cyclic voltammograms of a) acetylaminoferrocene (**1**) b) **1** + 1 equiv $(n\text{-Bu})_4$NSEt and c) **1** and 10 equiv $(n\text{-Bu})_4$NSEt in the solid state.

Table 6. Calculated Bond Order of Hydrogen Bonds in Acylaminoferrocene, $[(C_5H_5)Fe(C_5H_4NHCOR)]$, Using the Dimeric Models

	R	H···O
1	CH_3 long[a)]	0.09556
	CH_3 short[a)]	0.11301
2	CH_2CH_3	0.07903
3	*t*-Bu long[a)]	0.05922
	t-Bu short[a)]	0.07883
4	CF_3	0.05861

a) The dimeric model linked by the longer NH···O hydrogen bonds is expressed by "long" and the other is "short".

by ab initio calculation using the 3-21G(*) basis set. The calculated bond orders are summarized in Table 6, where two crystallographically distinct dimeric molecules were used for **1** and **3**. The bond orders of H···O for **1** are significantly large, a finding that is in agreement with the results of X-ray, spectral and electrochemical analyses. For **2**, the bond order is relatively large. These results suggest that all of the molecules in **1** and **2** are connected by continuous strong H···O bonds, which means that the hydrogen bonds are neither weak nor broken at any point. In the crystal of **3**, the long and short hydrogen bonds array alternatively. The bond order of the H···O=C hydrogen bond in the short one is comparable to that of **2**, but the long one exhibits a small bond order. The presumable hydrogen bond chains in **3** are essentially weakened, or broken.

Contribution of Electron Hopping to the Cyclic Voltammograms. Generally, long electron transfer occurs by super-exchange (electron tunneling), or electron-hopping mechanisms.[44,45] Recent studies have revealed that hydrogen bonds in the 3_{10}-helix promote an efficient electron transfer,[45] and that a suitable array of aromatic rings along the helical peptide increases the electron hopping.[46] In our case, a remarkable difference of cyclic voltammograms between **2** and **3** was observed despite an unclear spectral contrast between the hydrogen bonds. To elucidate this point, the electron-hopping

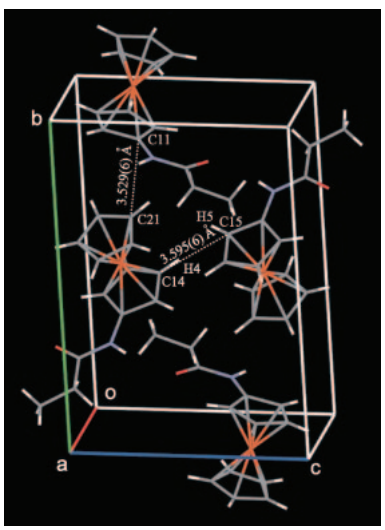

Fig. 7. Intermolecular contacts of $[(C_5H_5)Fe(C_5H_4\text{-}NHCOC_2H_5)]$ (**2**) in the crystal.

mechanism has been considered. Figure 7 shows the crystal packing of **2**. Intermolecular short contacts, C14···C15 (3.595(6) Å) and C11···C21 (3.529(6) Å), are found. The short Cp···Cp contact, where H4···H5 is 2.309 Å, probably functions as an effective pathway by a hopping mechanism, or π-conjugation. Each molecule is connected by hydrogen bonds to the adjacent molecules forming a continuous and expanded π-electron system. On the other hand, the shortest intermolecular Cp···Cp contact in the crystal of **3** is C22···C33 (3.79(1) Å), where the Cp rings are almost perpendicular to each other, and too far to interact effectively, resulting in isolated hydrogen bonds.

Conclusion

Acylaminoferrocenes, $[(C_5H_5)Fe(C_5H_4NHCOR)]$, were found to form characteristic intermolecular NH···O=C hydrogen-bond chains for which the bond strength depends quite

effectively on the substituent, R. The orientation of the amide proton with respect to the carbonyl group contributes to the strength of the hydrogen bonds. For R = CH_3 and CH_2CH_3, a unique electron transfer was detected critically by cyclic voltammetry in the solid state in terms of a large current and an irreversible redox process. Ferrocene derivatives having such strong hydrogen bonds are useful components to construct and strategically develop supramolecules with electronic properties. Such a combination of metal complexes with strong hydrogen-bond chains will widely expand applications, and will lead to the development of a new type of electronic devices (e.g., semi-conductor with a regulative path for electron transfer).

This work was supported by a Grant-in-Aid from the Ministry of Education, Culture, Sports, Science and Technology.

References

1 R. Rulkens, A. J. Lough, I. Manners, S. R. Lovelace, C. Grant, and W. E. Geiger, *J. Am. Chem. Soc.*, **118**, 12683 (1996).
2 J.-M. Lehn, "Supramolecular Chemistry—Concepts and Perspectives," VCH, Tokyo (1995).
3 J. C. MacDonald and G. M. Whitesides, *Chem. Rev.*, **94**, 2383 (1994).
4 G. R. Desiraju, *Angew. Chem., Int. Ed. Engl.*, **34**, 2311 (1995).
5 G. R. Desiraju, *Acc. Chem. Res.*, **29**, 441 (1996).
6 C. B. Aakeröy and K. R. Seddon, *Chem. Soc. Rev.*, **22**, 397 (1993).
7 D. Philp and J. F. Stoddart, *Angew. Chem., Int. Ed. Engl.*, **35**, 1154 (1996).
8 A. D. Burrows, C.-W. Chan, M. M. Chowdgry, J. E. McGray, and D. M. P. Mingos, *Chem. Soc. Rev.*, **24**, 329 (1995).
9 D. Braga, F. Grepioni, and G. R. Desiraju, *J. Organomet. Chem.*, **548**, 33 (1997).
10 T. Okamura, K. Sakauye, N. Ueyama, and A. Nakamura, *Inorg. Chem.*, **37**, 6731 (1998).
11 T. Okamura and N. Ueyama, "Metal-Hydrogen Bond Conjugated Systems," ed by A. Nakamura, N. Ueyama, and K. Yamaguchi, Kodansha, Tokyo (2002), pp. 307–330.
12 M. C. Grossel, M. R. Goldspink, J. A. Hriljac, and S. C. Weston, *Organometallics*, **10**, 851 (1991).
13 K. Kavallieratos, S. Hwang, and R. H. Crabtree, *Inorg. Chem.*, **38**, 5184 (1999).
14 D. v. Leusen and B. Hessen, *Organometallics*, **20**, 224 (2001).
15 P. D. Beer, F. Szemes, V. Balzani, C. M. Sala, M. G. B. Drew, S. W. Dent, and M. Maestri, *J. Am. Chem. Soc.*, **119**, 11864 (1997).
16 P. D. Beer, A. R. Graydon, A. O. M. Johnson, and D. K. Smith, *Inorg. Chem.*, **36**, 2112 (1997).
17 J. D. Carr, L. Lambert, D. E. Hibbs, M. B. Hursthouse, K. M. A. Malik, and J. H. R. Tucker, *J. Chem. Soc., Chem. Commun.*, **1997**, 1649.
18 K. Heinze and M. Schlenker, *Eur. J. Inorg. Chem.*, **2004**, 2974.
19 D. W. Hall and J. H. Richards, *J. Org. Chem.*, **28**, 1549 (1963).
20 T. Okamura, S. Takamizawa, N. Ueyama, and A. Nakamura, *Inorg. Chem.*, **37**, 18 (1998).
21 N. Ueyama, N. Nishikawa, Y. Yamada, T. Okamura, S. Oka, H. Sakurai, and A. Nakamura, *Inorg. Chem.*, **37**, 2415 (1998).
22 N. Ueyama, N. Nishikawa, Y. Yamada, T. Okamura, and A. Nakamura, *Inorg. Chim. Acta*, **283**, 91 (1998).
23 N. Ueyama, Y. Yamada, T. Okamura, S. Kimura, and A. Nakamura, *Inorg. Chem.*, **35**, 6473 (1996).
24 N. Ueyama, T. Okamura, and A. Nakamura, *J. Am. Chem. Soc.*, **114**, 8129 (1992).
25 N. F. Zakharchuk, B. Meyer, H. Hennig, F. Scholz, A. Jaworksi, and Z. Stojek, *J. Electroanal. Chem.*, **398**, 23 (1995).
26 A. Dostal, B. Meyer, F. Scholz, U. Schröder, A. M. Bond, F. Marken, and S. J. Shaw, *J. Phys. Chem.*, **99**, 2096 (1995).
27 A. Dostal, U. Schröder, and F. Scholz, *Inorg. Chem.*, **34**, 1711 (1995).
28 A. M. Bond, R. Colton, F. Daniels, D. R. Fernando, F. Marken, Y. Nagaosa, R. F. V. Steveninck, and J. N. Walter, *J. Am. Chem. Soc.*, **115**, 9556 (1993).
29 A. M. Bond, R. Colton, F. Marken, and J. N. Walter, *Organometallics*, **13**, 5122 (1994).
30 F. Scholz and B. Meyer, *Chem. Soc. Rev.*, **23**, 341 (1994).
31 S. Kitagawa, S. Matsuyama, M. Munakata, N. Osawa, and H. Masuda, *J. Chem. Soc., Dalton Trans.*, **1991**, 1717.
32 G. M. Scheldrick, "Crystallographic Computing 3," Oxford University Press (1985), pp. 175–189.
33 G. M. Scheldrick, "SHELXL97, Program for the Refinement of Crystal Structures," University of Göttingen, Germany (1997).
34 D. T. Cromer, "International Tables for X-ray Crystallography," T. K. Press, Birmingham, England (1974).
35 G. R. Knox, P. L. Pauson, D. Willison, E. Solčániová, and S. Toma, *Organometallics*, **9**, 301 (1990).
36 L. Leiserowitz and M. Tuval, *Acta Crystallogr.*, **B34**, 1230 (1978).
37 H. Adalsteinsson, A. H. Maulitz, and T. C. Bruice, *J. Am. Chem. Soc.*, **118**, 7689 (1996).
38 R. Taylor and O. Kennard, *Acc. Chem. Res.*, **17**, 320 (1984).
39 R. Taylor and O. Kennard, *Acta Crystallogr.*, **B39**, 133 (1983).
40 I. Schnell, S. P. Brown, H. Y. Low, H. Ishida, and H. W. Spiess, *J. Am. Chem. Soc.*, **120**, 11784 (1998).
41 S. Lu, V. V. Strelets, M. F. Ryan, W. J. Pietro, and A. B. P. Lever, *Inorg. Chem.*, **35**, 1013 (1996).
42 A. M. Bond and F. Marken, *J. Electroanal. Chem.*, **372**, 125 (1994).
43 F. A. Schultz and T. Kuwana, *J. Electroanal. Chem.*, **10**, 95 (1965).
44 M. Sisido, S. Hoshino, H. Kusano, M. Kuragaki, M. Makino, H. Sasaki, T. A. Smith, and K. P. Ghiggino, *J. Phys. Chem. B*, **105**, 10407 (2001).
45 F. Polo, S. Antonello, F. Formaggio, C. Toniolo, and F. Maran, *J. Am. Chem. Soc.*, **127**, 492 (2005); S. Antonello, F. Formaggio, A. Moretto, C. Toniolo, and F. Maran, *J. Am. Chem. Soc.*, **125**, 2874 (2003).
46 K. Yanagisawa, T. Morita, and S. Kimura, *J. Am. Chem. Soc.*, **126**, 12780 (2004).